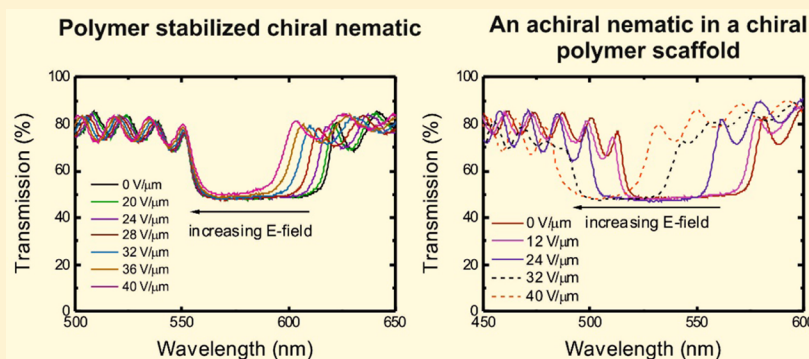# Macromolecules

Wavelength Tuning of the Photonic Band Gap of an Achiral Nematic Liquid Crystal Filled into a Chiral Polymer Scaffold

S. M. Wood, J. A. J. Fells, S. J. Elston, and S. M. Morris*

Department of Engineering Science, University of Oxford, Parks Road, Oxford OX1 3PJ, United Kingdom

ABSTRACT: We demonstrate electric-field-induced wavelength tuning of the entire photonic band gap of an achiral nematic liquid crystal (LC) filled into a chiral polymer scaffold. This chiral polymer scaffold has been formed by creating a template of a chiral nematic LC phase, which remarkably does not compromise the optical finesse of the band gap when compared to that of a conventional, polymer-stabilized chiral nematic LC. We present results on the spectral shift and temporal evolution of the photonic band gap in the presence of an external ac electric field. It is shown that initially there is a rapid ($\tau \approx 1$ ms) blue-shift of the long-wavelength band-edge followed by a considerably slower blue-shift ($\tau \approx 6.5$ s) of the entire band gap. We compare the results with those obtained for a polymer-stabilized chiral nematic LC where only a blue-shift of the long-wavelength band-edge is observed. Consequently, we find that for the templated sample the tuning range is more than a factor of 2 greater than that observed for the polymer-stabilized chiral nematic LC for the same range of electric field amplitudes. It is also found that there is little in the way of hysteresis upon increasing and decreasing the applied electric field magnitude. Finally, we present experimental evidence that suggests that the blue-shift of the entire band gap is due to an additional tuning mechanism present only for the case of the templated samples. This is believed to be caused by a contraction of the pitch that results from a translational motion of the polymer network. The greater tuning range observed in these templated samples is potentially important for the development of tunable 1-dimensional photonic band gaps and LC lasers. Furthermore, it avoids the use of dc electric fields that can lead to long-term issues regarding stability.

1. INTRODUCTION

The chiral nematic liquid crystal (LC) mesophase is characterized by macroscopic helices that spontaneously self-assemble due to the presence of chiral molecules. The helical arrangement of the liquid crystalline molecules has a periodicity that is equivalent to half of the pitch, p, of the helix, which is the length scale over which the director completes a full revolution of 2π. The pitch of a chiral nematic LC typically ranges in magnitude from a few hundred nanometers up to several micrometers. When viewed along the axis of the helix, these LC phases exhibit a vivid Bragg reflection band that reflects only one-handedness of circularly polarized light when the pitch is on the order of the wavelength of light.[1] The existence of this photonic band gap has been of paramount importance in applying chiral nematic LCs to a wide variety of technologies such as thin-film lasers, reflective displays, and tunable optical filters/mirrors.[2−4]

The spectral properties of the band gap, such as the wavelengths of the band-edges, are neatly represented by two simple relationships. Explicitly, these can be written as[5,6]

$$\lambda_L = n_\| p \tag{1}$$

$$\lambda_S = n_\perp p \tag{2}$$

where λ_X is the wavelength-position of the long ($X = L$) or short ($X = S$) band-edge of the reflection band, and $n_\|$ and $n_\perp$ are the refractive indices parallel and perpendicular to the director, respectively. These equations clearly illustrate that the wavelengths of the band-edges can be adjusted by altering either the relevant refractive index or the pitch of the helix. Since these parameters are sensitive to a range of external stimuli, this means that there are numerous routes by which the

wavelength of the band gap may be "tuned". For example, research has shown that the pitch of the helix may be changed using mechanical forces,[7] light,[8] and magnetic[9] and electric fields[10−12] whereas studies have shown that the relevant refractive indices may be changed using temperature[13] and electric fields.[14−25]

Of these various forms of external stimuli, electric fields are perhaps the most desirable option from a technological standpoint. However, the use of electric fields is complicated because the actual response of a chiral nematic LC to an externally applied electric field depends upon a number of factors. Specifically, this includes the orientation of the electric field direction relative to the helix axis ($\mathbf{h}$) and the sign of the dielectric anisotropy ($\Delta\varepsilon$).

One possible approach to tuning the reflection band is to lengthen the pitch by unwinding the structure using an electric field that is applied perpendicular to the axis of the helix (E⊥$\mathbf{h}$ and $\Delta\varepsilon > 0$). However, realizing this experimentally using conventional glass cells is nontrivial since only the standing helix geometry can be aligned to a high degree of uniformity. Consequently, to satisfy the requirement that the field direction is perpendicular to the helix axis (E⊥$\mathbf{h}$), interdigitated electrodes are thus required. Unfortunately, this leads to an inhomogeneous electric field profile around the electrodes and results in a nonuniform change in the helicoidal structure. This nonuniform electric field profile manifests as a degradation of the optical finesse of the band gap.[11] Furthermore, an electric field applied perpendicular to the helix axis can also lead to flexo-electric coupling, resulting in other modifications to the helical structure.[12]

In contrast, if an electric field is applied parallel to the helix axis (E∥$\mathbf{h}$) of a positive dielectric anisotropy chiral nematic LC ($\Delta\varepsilon > 0$), the Grandjean alignment collapses into a focal conic texture above a certain electric field amplitude.[14] This then leads to a subsequent loss of the photonic band gap when viewed along the normal of the glass substrates. In an attempt to maintain the geometry of a standing helix while using conventional planar electrodes at both substrates and still achieve wavelength tuning of the band gap, different methodologies have been explored.[10,14−22] For example, studies include using dc electric fields applied to chiral nematic LCs with a negative dielectric anisotropy ($\Delta\varepsilon < 0$) to exploit an electromechanical effect,[15,16] doping ferroelectric LC compounds into chiral nematic LCs,[17] using electrically commanded surfaces,[18] or using the heliconical structure that can be observed in dimeric LCs whereby the bend elastic constant, K_3, is much smaller than the twist elastic constant, K_2.[19]

One method for stabilizing the standing helix geometry in the presence of an external electric field involves using reactive mesogens to form a polymer network that "locks in" the alignment and prevents it from collapsing into a focal conic texture at high electric field amplitudes. This can either involve dispersing low concentrations of polymer by weight (<10 wt %), commonly referred to as polymer-stabilized LCs,[20] or higher concentrations (>10s of wt %) where the polymer forms more of a dense matrix consisting of micro- and nano-sized pores that contain the nonreactive LC components.[21−25] The nature of these pores is determined by a combination of the reactive mesogen concentration and the photocuring conditions (including the temperature at which the network is formed).[21] It has been shown that these structures are robust to high electric fields and that the reflection band can be tuned across a broad range of wavelengths (up to 141 nm has been

reported[22]) and with a fast relaxation (field ON−OFF) response time (as low as 10 μs[23]).

Alternatively, research has shown that the chiral LC component can be removed from these polymer network structures using a solvent and then replaced with an achiral nematic LC. Upon refilling the nematic LC into the polymer scaffold, it is then observed that a band gap can be retrieved even if there is no chirality present in the guest LC component.[26,27] These so-called polymer-templated devices have been used for the purposes of tuning the wavelength of the band gap, both by refilling with nematic LCs that had different properties to the host chiral nematic that was used to form the network[28] and by applying electric fields to the resulting structure.[27] In the latter case, some form of tuning was achieved by reorienting the LC molecules within the chiral polymer scaffold. However, the quality of the band gap was rather poor and was likely degraded by the washing-out/refilling process. Therefore, the tuning in this case is somewhat unclear because the band gap appears to collapse.

From previous studies, it does appear that the electro-optic properties for the polymer-templated samples are somewhat different than those of a conventional polymer-stabilized chiral nematic LC and that there is potential for wavelength tuning. Therefore, toward this end, we attempt to carry out a systematic study of the electro-optic properties of polymer-templated samples that possess a well-defined band gap and compare the behavior with that of a conventional polymer-stabilized chiral nematic LC. In so doing, we demonstrate analog wavelength tuning of the band gap using ac rather than dc electric fields and, more importantly, find that the templated samples exhibit a larger (by 2.5 times) tuning range of the long-wavelength band-edge with a lower electric field threshold. Overall, however, the tuning process takes substantially longer for the templated samples when compared to the polymer-stabilized chiral nematic LC (for the same range of electric field amplitudes). Additionally, the templated samples exhibit tuning of the entire band gap, while the polymer-stabilized samples only appear to exhibit tuning of the long wavelength band-edge. Consequently, we find that the electro-optic behavior is clearly different for the two types of devices, and we seek to provide a possible explanation for the physical mechanism responsible for tuning in each case.

2. EXPERIMENTAL METHODS

2.1. Sample Preparation. To form the base chiral nematic LC mixture consisting of nonreactive components, the high twisting power, sorbitol-based chiral dopant, R5011 (2.7 wt %, Merck KGaA), was dispersed into the achiral nematic LC, MDA-02-2149 (Merck KGaA), chosen because it exhibits a nematic phase at room temperature and has a high dielectric anisotropy of $\Delta\varepsilon = 38$ at $f = 1$ kHz with refractive indices of $n_\perp = 1.506$ and $n_\parallel = 1.686$ at a wavelength of ($\lambda = 633$ nm). MDA-02-2149 is a proprietary mixture of superfluorinated compounds. The resultant mixture produced a chiral nematic LC phase at room temperature ($p \sim 360$ nm) with a right-handed helix, as confirmed by polarizing optical microscopy. To study the effect of the polymer concentration on the electro-optic and templating properties, eight samples consisting of different concentrations by weight of the reactive mesogen mixture (0−80 wt %) were prepared. In particular, this allowed us to compare the effect of polymer concentration on the wavelength tuning ranges of the polymer-stabilized samples before carrying out the templating procedure. The reactive mesogen mixture used in this study (UCL-011-K1, Dai Nippon Ink) consisted of both mono- and diacrylates, a photoinitiator, and a thermal inhibitor. The mixtures were held above the clearing temperature of the LC (110 °C) for 16 h to allow for
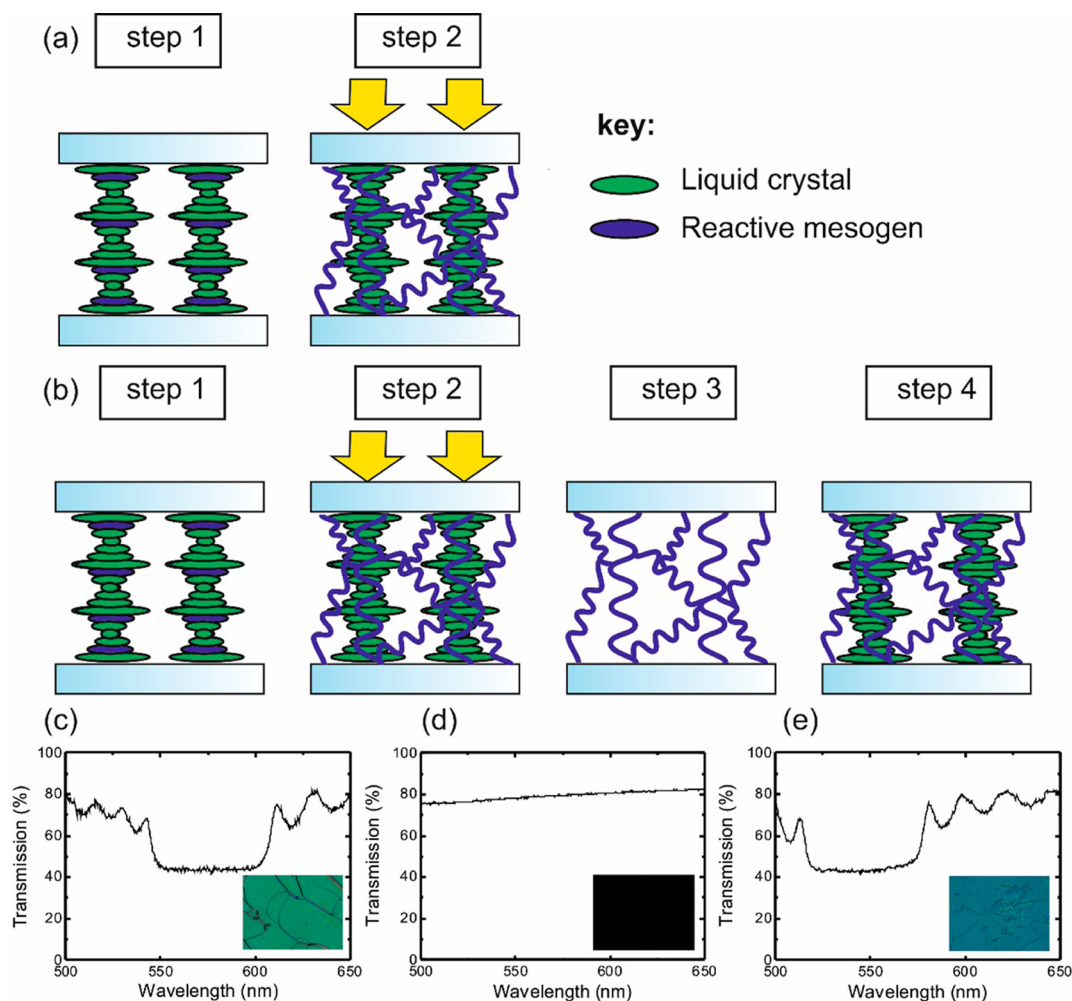
Figure 1. An illustration of the two different sample preparation techniques used in this study along with corresponding transmission spectra and microscope images at various stages of the fabrication process: (a) a conventional polymer-stabilized LC sample is created by filling a chiral nematic LC-reactive mesogen mixture into a glass cell (step 1) before exposure to UV light to form the polymer network (step 2); (b) a templated chiral polymer scaffold with an achiral nematic LC is formed by filling a chiral nematic LC-reactive mesogen mix into a glass cell (step 1) and then photopolymerized using UV light (step 2); the LC and remaining unreacted reactive mesogens are then removed to leave a chiral polymer scaffold (step 3), which is then refilled with an achiral nematic LC (step 4). Transmission spectrum after polymer stabilization (c), after removal of the non-cross-linked LC molecules (d), and after refilling the polymer scaffold with an achiral nematic LC (e).

thermal diffusion of the chemical constituents. All materials were used as received from the suppliers without any further purification.

To begin with, the mixtures were capillary-filled into 5 μm thick commercially available glass cells (Instec) that consisted of antiparallel rubbed polyimide alignment layers that were coated onto the inner substrates of the cell. To form a uniform standing helix (Grandjean) alignment, the samples were cooled from the isotropic phase and, if necessary, were subjected to mechanical shearing by applying pressure to give a good monodomain alignment. This alignment could be seen from both the optical polarizing microscope images and a band gap that had well-defined edges in the corresponding transmission spectrum for white light.

Following the alignment process, the samples were then illuminated at a wavelength of λ = 365 nm and an output power density of 185 mW/cm^2 at the light source, which was held at a distance of 20 cm away from the sample. To ensure uniform curing conditions, each sample was illuminated for 12 s on each side of the cell using a commercially available UV light source (Thorlabs CS2010). This procedure is illustrated in Figure 1a, and the corresponding transmission spectrum and optical texture observed on a polarizing microscope following the photopolymerization procedure are shown in Figure 1c.

To create the templated samples, the polymer-stabilized chiral nematic LC cells described above were washed out using acetone to remove both the unreacted monomer species and the LC molecules. For this step (step 3, Figure 1b), the samples were immersed in a beaker of acetone for 48 h and were then left to dry at room temperature for 4 h. The washed-out cells were examined on a microscope and spectrometer to confirm that the initial LC components had been removed (Figure 1d). The cells were then refilled with the achiral nematic LC, MDA-02-2149 by capillary action (step 4, Figure 1b). The refilling process for the templated samples was found to take significantly longer than the initial filling process, and therefore the cells were left at 110 °C for 24 h to ensure thorough filling of the LC into the porous polymer network. An example of the transmission spectrum demonstrating the reappearance of the band gap upon refilling the polymer scaffold with a nematic LC is shown in Figure 1e.

2.2. Spectral Analysis of the Band Gap. To obtain the transmission spectrum for each sample so as to observe the band gap, samples were illuminated by an unpolarized halogen white light source (Ocean Optics HL-2000-FHSA) focused to a spot size of $\approx$500 μm diameter at the sample using a 20×, 0.5 NA microscope objective. The transmission spectra were then collected by a 600 μm diameter optical fiber with an achromatic collection lens that was connected to a
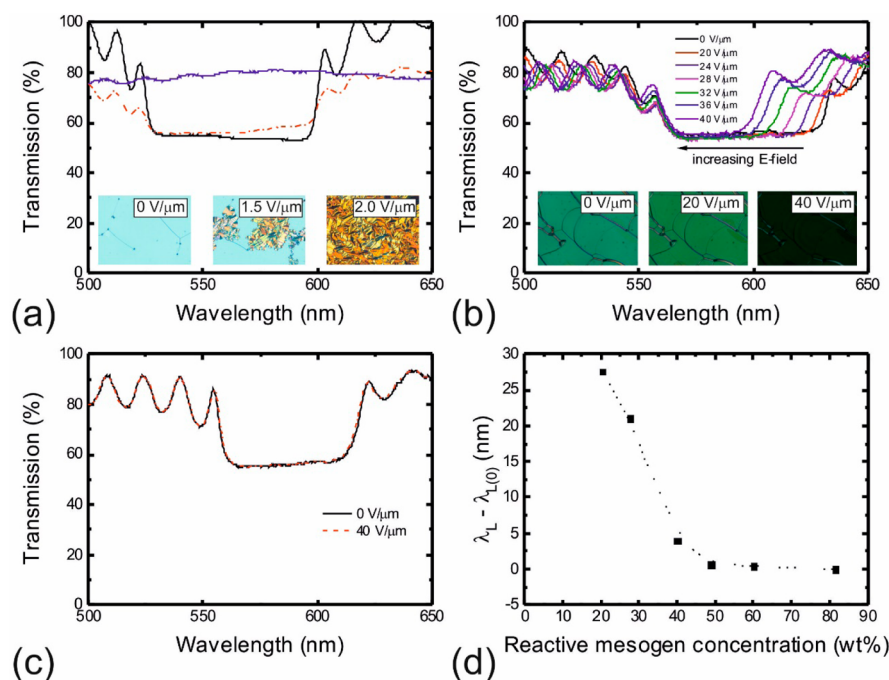
Figure 2. Effect of the reactive mesogen concentration on the wavelength tuning range of the photonic band gap of a polymer-stabilized chiral nematic LC. (a) The transmission spectrum for white light showing the collapse of the band gap as an E-field is applied to a chiral nematic LC sample without any reactive mesogen. The legend for the plot is as follows: $E = 0$ V/μm (black line), $E = 1.5$ V/μm (red, dashed line), $E = 2.0$ V/μm (blue line) (insets: polarizing microscope images showing the transformation of the Grandjean texture to a focal conic texture). (b) A blue-shift in the band gap for a chiral nematic LC sample consisting of 20 wt % reactive mesogen as the magnitude of the applied E-field is increased (inset: polarizing microscope images for three different E-field amplitudes). (c) The transmission spectrum for a chiral nematic LC sample consisting of 50 wt % reactive mesogen. (d) The maximum blue-shift of the long wavelength band-edge (λ_L) of the band gap as a function of the reactive mesogen concentration (by weight).

broadband spectrometer (Ocean Optics USB2000+ UV−vis; resolution 1.7 nm). To check the alignment and observe the change in the optical texture upon the application of an electric field, we used an Olympus BX51 optical polarizing microscope that was fitted with a color camera (QImaging QIcam Fast1394; 12-bit, color, 1392 × 1040 pixels) in the phototube.

2.3. Application of an Electric Field. An electric field was applied across the glass cells using two bipolar square-wave signals in antiphase. These signals were created by splitting a 1 kHz (up to 20 V$_{p-p}$) signal from a function generator (Tektronix AFG-3022) into two separate signals and passing one through a unity gain inverting amplifier to provide two complementary outputs with a common ground. Each output was amplified using a two-channel voltage amplifier (FCC electronics F10AP) to 200 V$_{p-p}$. One output was connected to one electrode and the complementary output connected to the other electrode of the glass cell to provide a combined voltage across the cell of up to 400 V$_{p-p}$ at 1 kHz (equivalent to an E-field of 40 V$_{rms}$/μm for 5 μm cells). The signals from the amplifier were monitored using a digitizing oscilloscope (Tektronix TDS224) to ensure that the waveform was not distorted at large voltage amplitudes.

For the response time measurements, the sample was illuminated by either a 590 nm (polymer-stabilized sample) or 565 nm (polymer-templated sample) LED (Thorlabs M590L3 and M565L3). The function generator output was internally amplitude modulated (100% depth) with a square wave to provide a gated output of bursts of modulated E-field (up to 40 V/μm) interspersed with gaps of zero field. The optical response of the transmitted light was then measured using a fast photodiode (Thorlabs PDA55) connected to a 16-bit data acquisition card sampling at 50 kS/s (National Instruments PCI-6033E).

3. RESULTS

3.1. Wavelength Tuning the Band Gap of a Polymer-Stabilized Chiral Nematic LC. Initially, polymer-stabilized

samples containing different concentrations of the reactive mesogen mixture were prepared (0−80 wt %) in order to understand the influence of the polymer concentration on the resulting wavelength tuning range of the band gap. Examples of the transmission spectra and corresponding optical polarizing microscope images are shown in Figure 2 for different electric field amplitudes. It is known that in the absence of a polymer network no wavelength tuning of the band gap is observed,[14] as demonstrated in Figure 2a. This is because at relatively low E-fields ($E \approx 1.4$ V/μm) the Grandjean alignment of the chiral nematic LC collapses into a focal conic texture (as is evident from the inset of Figure 2a), and as a result, the band gap that is observed at normal incidence disappears.

At polymer concentrations of 20 wt % and above, the Grandjean texture of the chiral nematic LC phase is stabilized by the polymer network and does not collapse into the focal conic state when a high-amplitude electric field is applied. We consider this concentration as an earlier report[27] using the same reactive mesogen mixture suggested that 25 wt % was required for the templating process. As an example, Figure 2b shows that as the electric field is increased, the long wavelength band-edge is blue-shifted continuously above a threshold E-field of 20 V/μm; this shift in the band-edge is accompanied by a change in the color of the optical texture that was recorded on the optical polarizing microscope (inset of Figure 2b). For concentrations between 5 and 20 wt % stabilization of the Grandjean texture was also observed with various degrees of wavelength tuning. For both the concentration shown in Figure 2 and higher concentrations of the reactive mesogen mixture, no evidence of phase separation was observed in either the microscope images or the transmission spectra.

The overall extent of the blue-shift is found to decrease with increasing concentration of reactive mesogen until it is almost completely suppressed at concentrations above 50 wt % (Figure 2c). The decrease in tuning range with an increase in the concentration of reactive mesogen can be seen clearly in Figure 2d, where the largest shift in the band gap that is observed is for a mixture consisting of 20 wt % reactive mesogen. However, at this concentration it was found that the polymer network was not sufficiently robust that it could survive the washing-out procedure and be used effectively as a template for other achiral nematic LCs. By increasing the concentration of the polymer to 30 wt %, it was found that the sample was sufficiently rugged that the polymer network could survive the washing-out procedure and thus could be used as a template. Consequently, for the remainder of this study, we concentrate on samples that consist of 30 wt % of the reactive mesogen mixture.

Results for the polymer-stabilized chiral nematic sample consisting of 30 wt % polymer are presented in Figure 3. It can
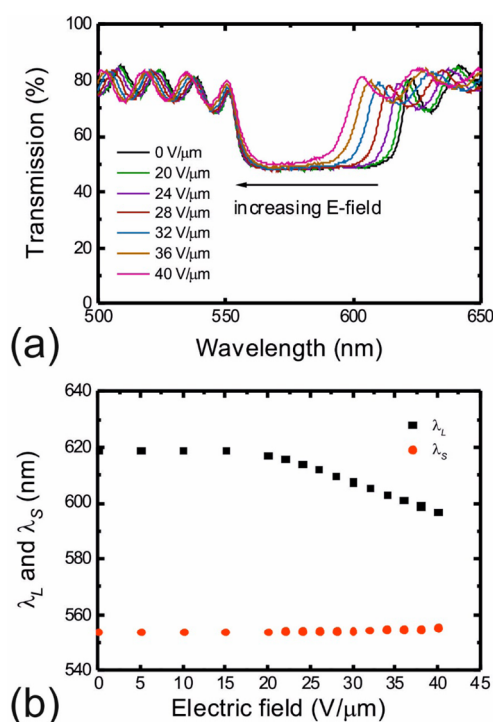

Figure 3. Wavelength tuning of the band gap for a polymer-stabilized chiral nematic LC with a concentration of reactive mesogen of 30 wt %. (a) The transmission spectra for different amplitudes of the applied electric field. (b) Plots of both the long- and short-wavelength band-edges as a function of the applied electric field.

be seen that during tuning the band gap maintains its integrity and sharp edges as the E-field increases (Figure 3a). The results show that above an approximate threshold of $E \approx 20$ V/μm the long band-edge blue-shifts from 619 to 597 nm (corresponding to a total shift of $\Delta\lambda_L = 22$ nm) for amplitudes up to $E = 40$ V/μm. On the other hand, there was no resolvable blue-shift in the short-band edge (Figure 3b), and therefore the overall width of the band gap was found to decrease from 65 to 43 nm.

Figure 4a shows the evolution with time of the transmission spectra after an E-field of 40 V/μm was applied to the sample. Within the first 100 ms, the long-wavelength band-edge was found to shift by its maximum extent while the short wavelength band-edge remained fixed and did not subsequently

change. This can be seen clearly in Figure 4b, in which the wavelengths corresponding to the band-edges are plotted as a function of time; initially, there is a relatively rapid shift in the long-wavelength band-edge (within the first 100 ms) which then remains static with a further increase in time after the electric field has been applied to the sample.

Figures 4a and 4b indicate that from the analysis of the transmission spectra the blue-shift occurs within a time scale of 100 ms. To determine the actual time required to respond to the electric field being applied and subsequently removed, measurements were carried out using an LED that emitted at a central wavelength that overlapped with the band gap of the chiral nematic LC sample. When the electric field was applied to the sample, the blue-shift of the long-wavelength band-edge resulted in an increase in the transmission intensity at the photodiode because the overlap between the emission spectrum of the LED and the band gap of the chiral nematic LC reduced. The voltage recorded on the photodiode is then plotted as a function of time as the electric field was modulated between 40 and 0 V/μm. This means that we can measure both the ON to OFF response time (the relaxation time) and the OFF to ON response time (the field-induced response time).

The relaxation time (ON−OFF) is perhaps a more useful metric to compare since it is well-known that this response time will be to a first-order approximation independent of the amplitude of the applied electric field. The response times are determined from the plots in Figure 4 and represent the 90% to 10% response time (relaxation time), and vice versa, for the response time recorded upon application of the external electric field. From Figure 4c, we find that the time required for the band gap to recover to its initial position was relatively fast, on the order of $\tau_{ON-OFF} \approx 1$ ms. In contrast, however, the time taken for the long-wavelength band-edge to blue-shift by its full extent was $\tau_{OFF-ON} \approx 8$ ms for an electric field of 40 V/μm (Figure 4d). It should be noted that these graphs show envelopes of an additional feature occurring at a 2 kHz frequency, which is twice that of the driving frequency of the applied electric field.

3.2. Wavelength Tuning of the Band Gap of an Achiral Nematic LC in a Chiral Polymer Scaffold. Having characterized the polymer-stabilized chiral nematic samples, our next step was to prepare the templated samples. To this end, a chiral polymer scaffold was created from the same 30 wt % mixture as described in the Sample Preparation section. Figure 5a shows the change in the transmission spectrum of the templated samples following the application of an external electric field. In a similar manner to that observed for the polymer-stabilized samples, the band gap was retained even with an increase in the electric field amplitude. However, in this case, both the long- and short-wavelength band-edges (λ_L and λ_S) blue-shift as the electric field amplitude increases. During the wavelength tuning process, the optical finesse of the band gap is largely maintained, and there is minimal hysteresis upon increasing and decreasing the electric field amplitude (inset of Figure 5a). It should be noted that due to the refilling procedure, the photonic band gap is not located at exactly the same wavelengths as that observed for the polymer-stabilized chiral nematic LC. This could be due to slight differences in the refractive indices between the achiral nematic LC filled into the template and the original chiral nematic mixture.

Accompanying the shift in the band gap, there is also a change in the optical texture that is observed when viewed on an optical polarizing microscope—in this case the image
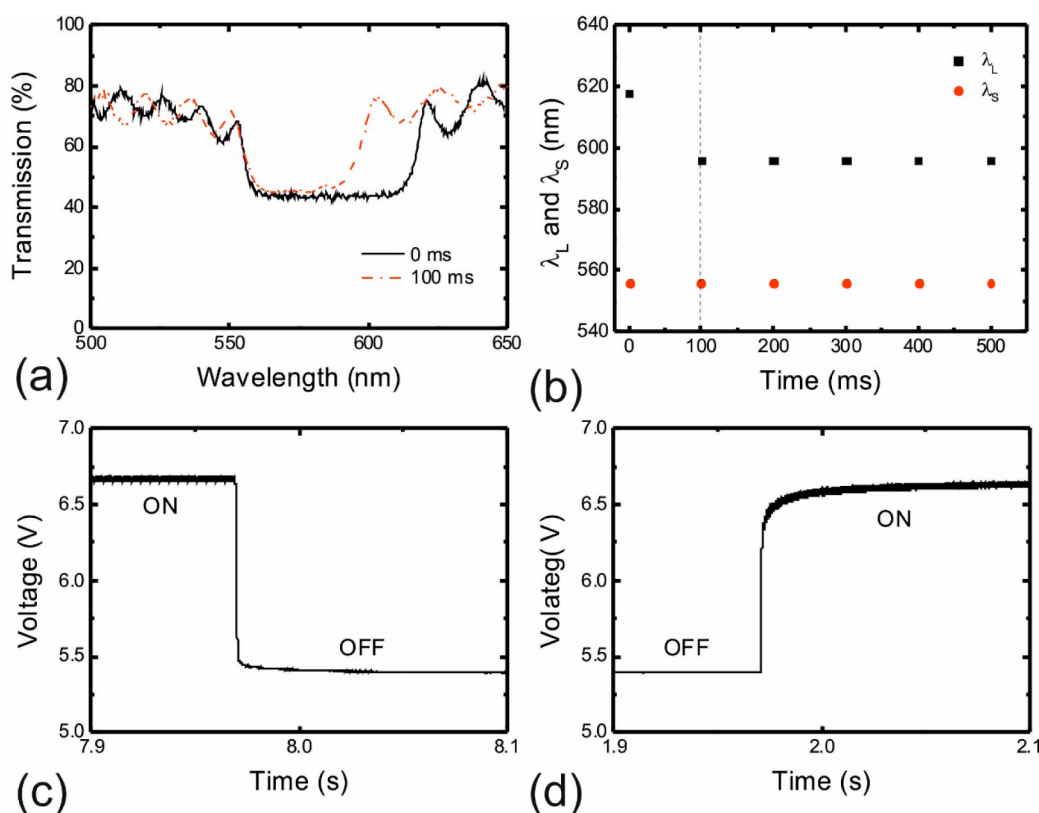
Figure 4. Time required for wavelength tuning of the band gap of a polymer-stabilized chiral nematic LC consisting of 30 wt % reactive mesogen. In this case an electric field of 20 V/μm was applied to the sample and was maintained during measurements. (a) The blue-shift of the transmission spectrum after the electric field had been applied for 100 ms. (b) The wavelengths of the long- and short-wavelength band-edges as a function of time following the application of the electric field. The change in transmitted intensity recorded on the photodiode following the removal (c) and the application (d) of the applied electric field.

changes to a darker green commensurate with the shift in the reflection band in the red−yellow region of the spectrum. In addition to the conventional Grandjean texture, a random configuration of bright stripes appear as the electric field amplitude is increased, which is discussed in more detail in the next section. Figure 5b shows the change in each band-edge with increasing electric field amplitude. In this case, the long band-edge evidently shifts by a greater amount than that observed for the short band-edge ($\Delta\lambda_L$ = 55 nm compared with $\Delta\lambda_s$ = 32 nm).

Figure 6a shows the temporal evolution of the transmission spectrum over a time period of 5 s following the application of an E-field of 40 V/μm to the sample. It is clear that within the first 100 ms the templated sample exhibits a blue-shift of only the long wavelength band-edge and that after 100 ms there is then a subsequent blue-shift of the entire band gap. The wavelengths corresponding to the two band-edges are plotted separately in Figure 6b as a function of time following the application of an external electric field. These results show that, initially, the short wavelength band-edge is unchanged during the first 200 ms, which is commensurate with the behavior observed for the polymer-stabilized sample; this is then followed by a slower blue-shift of both band-edges that takes place over a time period of several seconds.

To measure the response time, an LED with a peak emission wavelength at 565 nm was used due to the slightly different spectral location of the photonic band gap; however, the measurement principle was identical to that used for the polymer-stabilized sample described in the previous subsection.

Figures 6c and 6d show the relaxation (E-field ON−OFF) and driven response time (E-field OFF−ON) for the sample, respectively. From these figures it can clearly be seen that the response times are substantially longer than that recorded for the polymer-stabilized sample. It takes $\tau_{ON-OFF} \approx 6.5$ s for the band gap to recover to its initial position when the electric field is removed and $\tau_{OFF-ON} \approx 2.8$ s for the band gap to blue-shift by the maximum extent when the electric field is applied. In both cases, there was an initial fast change in the voltage measured, followed by a slower, longer shift. For the relaxation time results in Figure 6c, the voltage on the photodiode dips below its final value before increasing when the voltage is removed. This is likely due to the interference fringes either side of the photonic band gap (i.e., the peaks and troughs in the transmission as can be seen in Figure 6a, for example). The wavelengths corresponding to these peaks appears to shift as a voltage is applied, and their positions will have an effect on the device transmission (and hence the voltage that we record). The τ_{ON-OFF} relaxation time is calculated as the time it takes for the voltage to drop from 90% of the initial value to 10% of the total change.

4. DISCUSSION

From our results, it is evident that the polymer-stabilized and templated samples exhibit different wavelength tuning characteristics of the band gap. For the polymer-stabilized sample, the long-wavelength band-edge appears to blue-shift by $\Delta\lambda_L \approx 22$ nm in a time scale on the order of milliseconds, and this is the only change that is observed for the electric field amplitudes
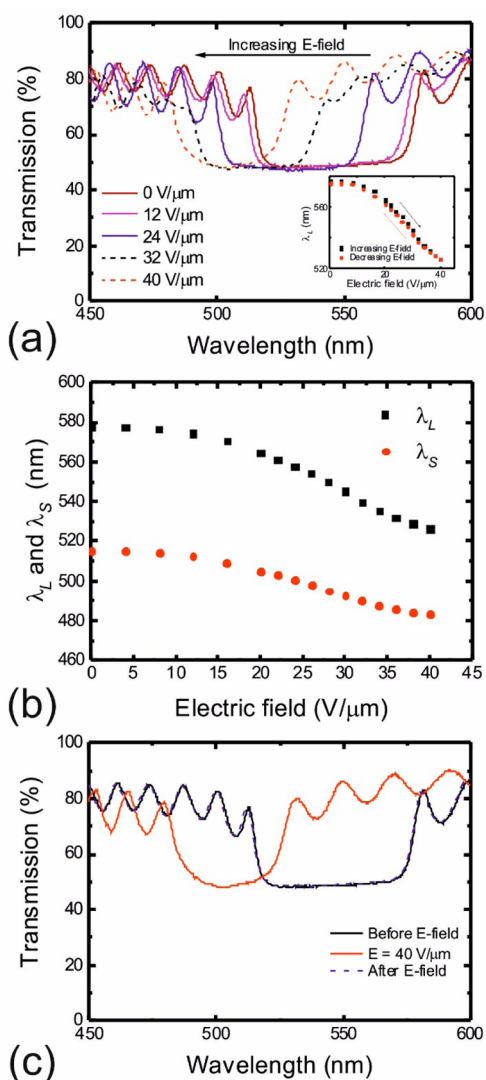
Figure 5. Wavelength tuning of the band gap for an achiral nematic LC filled into a chiral polymer scaffold. (a) The transmission spectrum recorded for different amplitudes of the applied electric field (inset: a plot of the long-wavelength band-edge upon increasing and decreasing the applied electric field). (b) Plots of both the long- and short-wavelength band-edges as a function of the applied electric field amplitude. (c) Transmission spectra before, during, and after the application of an electric field.

that are considered in this study. Interestingly, a similar blue-shift (of $\Delta\lambda_L \approx 22$ nm in a comparable time scale) is also seen in the case of the templated samples; however, there is then a further blue-shift of the entire band gap over a much longer time scale (an additional shift of $\Delta\lambda_L \approx 32$ nm on the order of seconds). Evidently, it appears as though both the polymer-stabilized and the templated samples behave in an identical manner initially but that the templated sample exhibits a secondary process involving a blue-shift of the entire band gap.

For the polymer-stabilized samples exhibiting the fast mechanism, the relaxation time is found to be faster than the field-induced response time. This is believed to be due to the additional restoring force that is provided by the polymer network. For the polymer-templated samples (where both the fast and the slow responses are observed), the field-induced response time is found to be faster than the relaxation time. This is considered to be the result of a weakening of the

polymer network in the templated samples that is caused by the washing-out and refilling procedure, which in turn leads to a smaller restoring force.

To begin to explain the two mechanisms responsible for the photonic band gap tuning, let us consider the first, fast process in which only the long wavelength band-edge blue-shifts by $\Delta\lambda_L \approx 22$ nm. This blue-shift occurs in a time period of $\tau \approx 8$ ms, and for the polymer-stabilized sample, no further movement of the band gap is observed. During this process, there is no apparent change in the Grandjean texture when viewed on an optical polarizing microscope apart from the slight change in the color as shown in the inset of Figure 2b and discussed in section 3.1. A blue-shift of λ_L in polymer-stabilized chiral nematic LCs has been observed previously[17,21−23] and has been attributed to a reduction in $n_\parallel$ while $n_\perp$ and p remain fixed. This change in the effective $n_\parallel$ is the result of a reorientation (tilt) of the interstitial LC molecules within the polymer network. Thus, from eqs 1 and 2, only the long-wavelength band edge is observed to blue-shift while the short band-edge remains unchanged. Our results are commensurate with those reported in the literature[21−23] (e.g., a 48 nm shift is seen for a mixture containing 40 wt % reactive mesogen when a 110 V/μm electric field is applied[22]). By using eq 1, we calculate that the wavelength tuning we observe in this study corresponds to a small change in $n_\parallel$ of $\delta n_\parallel \sim 0.06$.

The second mechanism that is observed, which is present only in the templated sample, results in an additional blue-shift of the long-wavelength band-edge (an extra $\Delta\lambda_L \approx 32$ nm), accompanied now by a blue-shift of the short-wavelength band-edge as well. This additional tuning of the band gap, which is very slow ($\tau_{ON-OFF} \approx 6.5$ s), indicates that as the entire band gap is seen to blue-shift, the pitch of the structure may be decreasing. In previous work on polymer-templated samples it was claimed that only the long band-edge of the band gap blue-shifted.[17] However, in ref 17, the refilling procedure resulted in a band gap that was somewhat degraded and therefore lacked well-defined band-edges, thus making it difficult to track the actual response. In this study, we are using exactly the same reactive mesogen mixture as that used in ref 27 and have also observed similar results to those presented here for other nematic LCs (such as E7) and other reactive mesogens (e.g., RM257). As a result, this makes it difficult to determine whether only one or both band-edges are changing. Further, in that work the long-wavelength band-edge was found to shift by $\Delta\lambda_L \approx 50$ nm when an E-field of $E = 43$ V/μm was applied to a sample comprising approximately 40 wt % polymer. In our study, we see a commensurate shift ($\Delta\lambda_L \approx 55$ nm for a 40 V/μm E-field applied to a sample containing approximately 30 wt % polymer).

The time scale over which the second mechanism operates suggests that a flow-related phenomenon may be involved. Given that both band-edges are seen to blue-shift, this would perhaps suggest that the pitch is changing, which is somewhat surprising given that one might expect the pitch to be "locked-in" by the polymer network. Evidence to the contrary has been presented in recent work[10,29−31] where it was shown that it is possible for the polymer fibrils that make up the network to undergo a translational motion when subjected to dc electric fields. This in turn leads to a contraction of the pitch at one substrate and an extension at the other when the polymer network is tethered to both substrates. The caveat is that this observation is only true for dc electric fields that are applied to a polymer stabilized chiral nematic LC with a negative dielectric
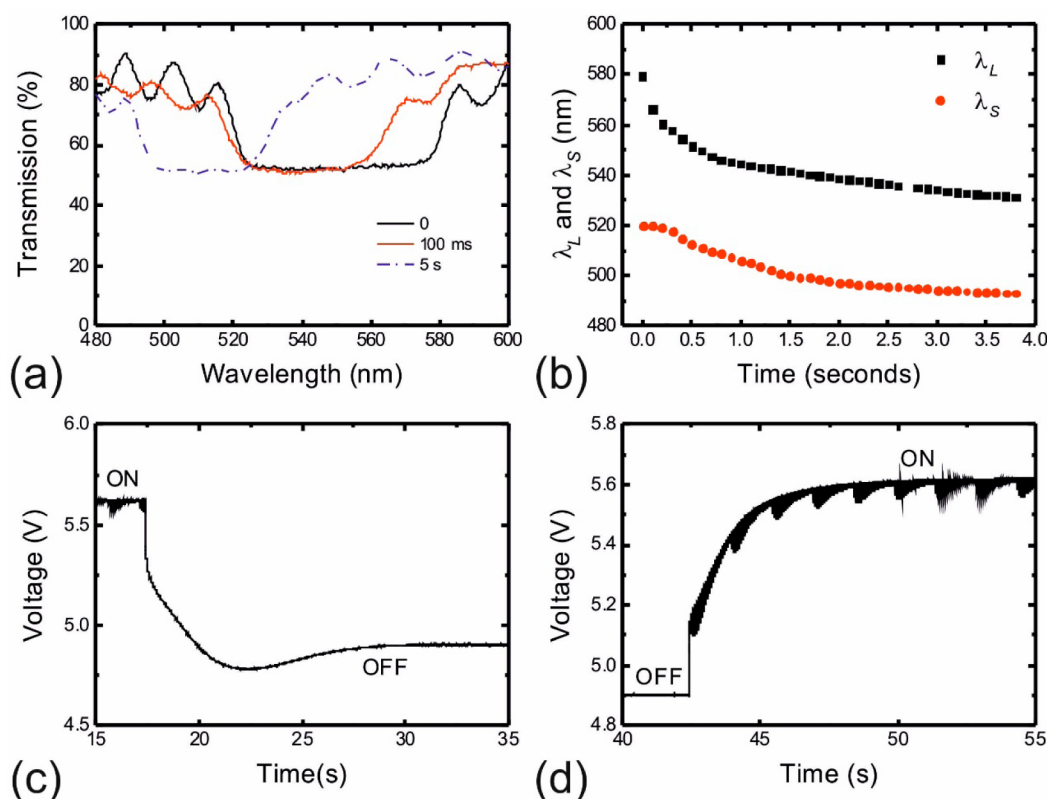
Figure 6. Time required for wavelength tuning of the band gap of an achiral nematic LC filled into a chiral polymer scaffold. In this case an electric field of 40 V/μm was applied to the sample and was maintained during measurements. (a) The blue-shift of the transmission spectrum after the electric field had been applied for 5 s. (b) The wavelengths of the long- and short-wavelength band-edges as a function of time following the application of the electric field. The change in transmitted intensity recorded on the photodiode following the removal (c) and the application (d) of the applied electric field.

anisotropy. For high frequency ac electric fields applied to a positive dielectric anisotropy polymer-stabilized LC, no translational motion of the polymer network was observed by the authors. In this case, only a tilting of the chiral nematic helix was observed.

Examples of polarizing microscope images of the templated sample are presented in Figure 7 in which we see additional features appearing as the amplitude of the E-field is increased. As the field is applied, streaks come in to focus that are much lighter in color than the surrounding regions. At this stage, it is unclear what these features are and whether they are related in some way to the additional and slow tuning mechanism. However, it should be stressed that such features were not observed in the polymer-stabilized samples across the same range of electric field amplitudes. One possibility is that these features could potentially be the polymer fibrils coming into focus as they translate through the cell or equally oily streaks, either of which could be driven by a flow of the nematic LC.

As we are using a high-frequency (1 kHz) electric field that is applied to a nematic LC with a positive dielectric anisotropy in this study, this indicates the possibility of a dielectrically driven process. This is potentially possible if (a) the polymer network is not strongly attached to at least one of the device surfaces and (b) diffusion and/or flow of the nematic LC material is possible through the polymer network, which would equally be true if the polymer structure is porous. We know the latter to be possible because the LC material has been refilled into the network template through a flow/diffusion process as part of the device formation. Additionally, if the process of washing-out

and refilling with a nematic material has to some degree "damaged" the polymer network, then it is also reasonable that it may no longer be strongly attached to the surfaces and/or that the porous regions have been enlarged. Evidence for a weakening of the network has already been seen from the slight degradation in the quality of the photonic band gap upon refilling with a nematic LC and in the samples using a low concentration (<30 wt %) of polymer which could not survive the washing/refilling process. It is therefore entirely possible that some of the fibrils that make up the network may have been broken in some places.

We can see from Figure 5a that the electric-field-induced tilt in the LC molecular axis within the polymer network does not reach the homeotropic state but remains partially tilted within the network structure: this is evident because the longer band edge blue-shifts but does not reach, or get very close, to the wavelength of the shorter band-edge. We postulate that at the highest electric field amplitudes used in this study, and after the initial tilting of the nematic LC within the polymer network, the LC material then flows/diffuses through the network to form a homeotropic region near one or both surfaces. In accordance, the polymer network region is then reduced in thickness, with a consequent reduction in the helix pitch. This is something that can occur for materials with a positive dielectric anisotropy only if the dielectric energy change associated with the formation of the homeotropic region is greater than the elastic energy cost of reducing the thickness of the polymer network region. To reduce the thickness of this region, the LC molecules must flow/diffuse into the homeotropic region(s) so as to conserve
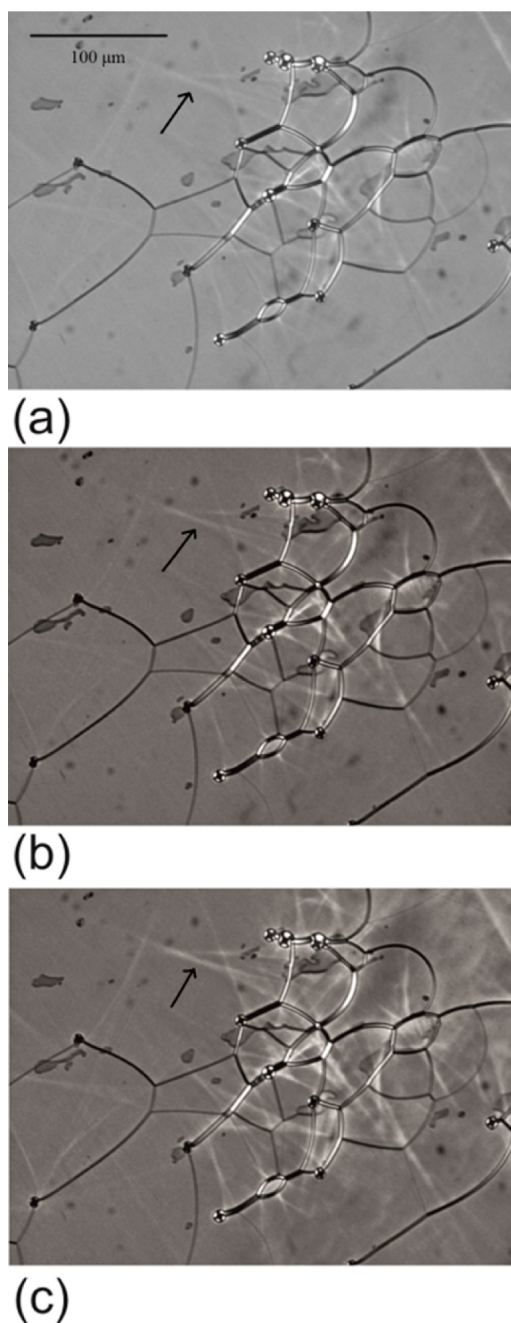
Figure 7. Optical polarizing microscopy images of an achiral nematic LC filled into a chiral polymer scaffold following the application of an ac electric field ($E = 40$ V/μm, $f = 1$ kHz): (a) 100, (b) 200, and (c) 300 ms after a 40 V/μm 1 kHz ac electric field is applied to the cell. The images have been grayscale mapped to improve the contrast, and the dark arrow in each image indicates additional features that come into focus with an increase in the applied electric field amplitude.

volume. As a diffusion/flow process is typically slow, this then fits with our measured response times. We also observe that upon removal of the applied electric field the band gap recovers to the initial position (see Figure 5c), and the additional features that were observed in the microscope images (Figure 7) then disappear out of focus and the initial, pre-electric field state is recovered. At sufficiently large fields it may be possible to induce further reorientation of the LC molecular axis, but within the field regime investigated in this study it appears that the elastic energy associated with such a further reorientation is

greater than that associated with flow of the LC material and consequent reorganization of the polymer network. Thus, it is the field interaction with the LC which appears to drive the potential reorganization of the polymer network rather than a field-induced translation of the polymer structure.

5. CONCLUSION

In this work, we have performed a systematic study on the wavelength tuning characteristics of the photonic band gap for an achiral nematic LC that is dispersed into a chiral polymer scaffold and compared it to that of a conventional, polymer-stabilized chiral nematic LC. By applying an ac electric field ($f = 1$ kHz) to a polymer-templated sample, we have observed a blue-shift of the photonic band gap by 55 nm when an E-field of $E = 40$ V/μm was applied. This tuning range is significantly greater (by 2.5 times) than that observed for a conventional polymer-stabilized chiral nematic LC. Our results indicate that the blue-shift appears to be composed of an initial, fast (≈ 1 ms) blue-shift of 22 nm of only the long-wavelength band-edge, followed by a slower blue-shift of 32 nm of the entire band gap. We have provided a potential explanation of the origins of these two effects in terms of a change in the effective refractive index of the LC as well as a contraction of the pitch as a result of a translation of the polymer fibrils. With further developments in the reactive mesogen mixtures and the photocuring conditions used to create the polymer scaffolds, it might be possible to achieve even faster response times and larger wavelength tuning ranges. Further research is required to fully understand the second tuning mechanism in detail as well as the role of the chiral dopant concentration and the polymer molecular weight on the resulting tuning range. These results are potentially important for the development of polymer-templated LC devices and in the design of tunable mirrors, filters, and LC lasers.

■ AUTHOR INFORMATION

Corresponding Author
*E-mail stephen.morris@eng.ox.ac.uk.

Notes
The authors declare no competing financial interest.

■ REFERENCES

(1) de Gennes, P. G.; Prost, J. P. *The Physics of Liquid Crystals*, 2nd ed.; Oxford University Press: Oxford, UK, 1995; Chapters 1 and 2.
(2) For a recent review see: Coles, H.; Morris, S. Liquid Crystal Lasers. *Nat. Photonics* **2010**, 4, 676−685.
(3) Kim, K.-H.; Song, J. K. Technical Evolution of Liquid Crystal Displays. *NPG Asia Mater.* **2009**, 1, 29−36.
(4) Woltman, S. J.; Jay, G. D.; Crawford, G. P. Liquid Crystals Find a New Order in Biomedical Applications. *Nat. Mater.* **2007**, 6, 929−938.
(5) de Vries, H. Rotary Power and Other Optical Properties of Certain Liquid Crystals. *Acta Crystallogr.* **1951**, 4, 219−226.
(6) Schmidtke, J.; Stille, W. Fluorescence of a Dye-doped Cholesteric Liquid Crystal Film in the Region of the Stop Band: Theory and Experiment. *Eur. Phys. J. B* **2003**, 31, 179−194.
(7) Finkelmann, H.; Kim, S. T.; Muñoz, A.; Palffy-Muhoray, P.; Taheri, B. Tunable Mirrorless Lasing in Cholesteric Liquid Crystalline Elastomers. *Adv. Mater.* **2001**, 13, 1069−1072.

(8) Kurihara, S.; Hatae, Y.; Yoshioka, T.; Moritsugu, M.; Ogata, T.; Nonaka, T. Photo-tuning of Lasing from a Dye-doped Cholesteric Liquid Crystals by Photoisomerization of a Sugar Derivative having Plural Azobenzene Groups. *Appl. Phys. Lett.* **2006**, *88*, 103121.

(9) Lelidis, I.; Barbero, G.; Scarfone, A. M. Cholesteric Pitch-transitions Induced by a Magnetic Field in a Sample Containing Incomplete Number of Pitches. *Cent. Eur. J. Phys.* **2012**, *10*, 587−593.

(10) Nemati, H.; Liu, S.; Zola, R. S.; Tondiglia, V. P.; Lee, K. M.; White, T.; Bunning, T.; Yang, D.-K. Mechanism of Electrically Induced Photonic Band Gap Broadening in Polymer Stabilized Cholesteric Liquid Crystals with Negative Dielectric Anisotropies. *Soft Matter* **2015**, *11*, 1208−1213.

(11) Schmidtke, J.; Jünnemann, G.; Keuker-Baumann, S.; Kitzerow, H.-S. Electrical Fine Tuning of Liquid Crystal Lasers. *Appl. Phys. Lett.* **2012**, *101*, 051117.

(12) Patel, J. S.; Meyer, R. B. Flexoelectric Electro-optics of a Cholesteric Liquid Crystal. *Phys. Rev. Lett.* **1987**, *58*, 1538−1540.

(13) Funamoto, K.; Ozaki, M.; Yoshino, K. Discontinuous Shift of Lasing Wavelength with Temperature in Cholesteric Liquid Crystal. *Jpn. J. Appl. Phys.* **2003**, *42*, 1523−1525.

(14) Furumi, S.; Yokoyama, S.; Otomo, A.; Mashiko, S. Electrical control of the structure and lasing in chiral photonic band-gap liquid crystals. *Appl. Phys. Lett.* **2003**, *82*, 16.

(15) Tondiglia, V. T.; Natarajan, L. V.; Bailey, C. A.; Duning, M. M.; Sutherland, R. L.; Ke-Yang, D.; Voevodin, A.; White, T. J.; Bunning, T. J. Electrically Induced Bandwidth Broadening in Polymer Stabilized Cholesteric Liquid Crystals. *J. Appl. Phys.* **2011**, *110*, 053109.

(16) Lu, H.; Hu, J.; Chu, Y.; Xu, W.; Qiu, L.; Wang, X.; Zhang, G.; Hu, J.; Yang, J. Cholesteric Liquid Crystals with an Electrically Controllable Reflection Bandwidth Based on Ionic Polymer Networks and Chiral Ions. *J. Mater. Chem. C* **2015**, *3*, 5406−5411.

(17) Choi, S. S.; Morris, S. M.; Huck, W. T. S.; Coles, H. J. Electrically Tuneable Liquid Crystal Photonic Bandgaps. *Adv. Mater.* **2009**, *21*, 3915−3918.

(18) Choi, S. S.; Morris, S. M.; Coles, H. J.; Huck, W. T. S. Wavelength Tuning the Photonic Band Gap in Chiral Nematic Liquid Crystals using Electrically Commanded Surfaces. *Appl. Phys. Lett.* **2007**, *91*, 231110.

(19) Xiang, J.; Li, Y.; Li, Q.; Paterson, D. A.; Storey, J. M. D.; Imrie, C. T.; Lavrentovich, O. D. Electrically Tunable Selective Reflection of Light from Ultraviolet to Visible and Infrared by Heliconical Cholesterics. *Adv. Mater.* **2015**, *27*, 3014−3018.

(20) Hikmet, R. A. M.; Kemperman, H. Electrically Switchable Mirrors and Optical Components Made from Liquid-Crystal Gels. *Nature* **1998**, *392*, 476−479.

(21) Kim, H.; Inoue, Y.; Kobashi, J.; Maeda, Y.; Yoshida, H.; Ozaki, M. Deformation-Free Switching of Polymer-Stabilized Cholesteric Liquid Crystals by Low Temperature Polymerization. *Opt. Mater. Express* **2016**, *6*, 705−710.

(22) Mohammadimasoudi, M.; Beeckman, J.; Shin, J.; Lee, K.; Neyts, K. Widely Tuneable Chiral Nematic Liquid Crystal Optical Filter with Microsecond Switching Time. *Opt. Express* **2014**, *22*, 19098−19107.

(23) Inoue, Y.; Yoshida, H.; Kubo, H.; Ozaki, M. Deformation-free Microsecond Electro-optic Tuning of Liquid Crystals. *Adv. Opt. Mater.* **2013**, *1*, 256−263.

(24) Yoshida, H.; Inoue, Y.; Shiozaki, Y.; Takahashi, M.; Kubo, H.; Fujii, A.; Ozaki, M. Fast and Continuous Tunable Lasing from a Nano-pore Embedded Cholesteric Liquid Crystal Film. *Mol. Cryst. Liq. Cryst.* **2012**, *560*, 101−107.

(25) Kim, H.; Kobashi, J.; Maeda, Y.; Yoshida, H.; Ozaki, M. Pitch-length Independent Threshold Voltage of Polymer/cholesteric Liquid Crystal Nano-composites. *Crystals* **2015**, *5*, 302−311.

(26) de Gennes, P. G. Possibilites Offertes Par la Reticulation de Polymeres en Presence d'un Cristal Liquide. *Phys. Lett. A* **1969**, *28*, 725−726.

(27) Choi, S. S.; Morris, S. M.; Huck, W. T. S.; Coles, H. J. Simultaneous Red-green-blue Reflection and Wavelength Tuning from an Achiral Liquid Crystal and a Polymer Template. *Adv. Mater.* **2010**, *22*, 53−56.

(28) Lin, J. D.; Chu, C.-L.; Lin, H.-Y.; You, B.; Horng, C.-T.; Huang, S.-Y.; Mo, T.-S.; Huang, C.-Y.; Lee, C.-R. Wide-band Tunable Photonic Bandgaps Based on Nematic-refilling Cholesteric Liquid Crystal Polymer Template Samples. *Opt. Mater. Express* **2015**, *5*, 1419−1430.

(29) Tondiglia, C. P.; Natarajan, L. V.; Bailey, C. A.; McConney, M. E.; Lee, K. M.; Bunning, T. J.; Zola, R.; Nemati, H.; Yang, D.-K.; White, T. J. Bandwidth Broadening Induced by Ionic Interactions in Polymer Stabilized Cholesteric Liquid Crystals. *Opt. Mater. Express* **2014**, *4*, 1465−1472.

(30) Lee, K. M.; Tondiglia, V. P.; McConney, M. E.; Natarajan, V.; Bunning, T. J.; White, T. J. Color-tunable Mirrors Based on Electrically Regulated Bandwidth Broadening in Polymer-stabilized Cholesteric Liquid Crystals. *ACS Photonics* **2014**, *1*, 1033−1041.

(31) Lee, K. M.; Tondiglia, V. P.; Lee, T.; Smalyukh, I. I.; White, T. J. Large Range Electrically-induced Reflection Notch Tuning in Polymer Stabilized Cholesteric Liquid Crystals. *J. Mater. Chem. C* **2015**, *3*, 8788−8793.